Path-based methods for the determination of nondispersive drainage directions in grid-based digital elevation models

Stefano Orlandini, Giovanni Moretti, and Marco Franchini

Dipartimento di Ingegneria, Università degli Studi di Ferrara, Ferrara, Italy

Barbara Aldighieri and Bruno Testa

Istituto per la Dinamica dei Processi Ambientali, Consiglio Nazionale delle Ricerche, Milan, Italy

[1]   Path-based methods for the determination of nondispersive drainage directions in grid-based digital elevation models are presented. These methods extend the descriptive capabilities of the classical D8 method by cumulating the deviations between selected and theoretical drainage directions along the drainage paths. It is shown that either angular or transversal deviations can be employed. Accordingly, two classes of methods designated D8-LAD (eight drainage directions, least angular deviation) and D8-LTD (eight drainage directions, least transversal deviation) are developed. Detailed tests on four synthetic drainage systems of known geometry and on the Liro catchment (central Italian Alps) indicate that the proposed methods provide significant improvement over the D8 method for the determination of drainage directions and drainage areas.   *INDEX TERMS:* 1848 Hydrology: Networks; 1824 Hydrology: Geomorphology (1625); 1894 Hydrology: Instruments and techniques; *KEYWORDS:* terrain analysis, drainage networks, drainage areas

Citation: Orlandini, S., G. Moretti, M. Franchini, B. Aldighieri, and B. Testa, Path-based methods for the determination of nondispersive drainage directions in grid-based digital elevation models, *Water Resour. Res.*, *39*(6), 1144, doi:10.1029/2002WR001639, 2003.

1. Introduction

[2] The earliest and simplest method for specifying drainage directions in grid-based digital elevation models (DEMs) is to assign a pointer from each cell to one of its eight neighbors, either adjacent or diagonal, in the direction of the steepest downward slope. This method was introduced by *O'Callaghan and Mark* [1984] and *Marks et al.* [1984] and is commonly designated D8 (eight drainage directions). The D8 approach has two major limitations: (1) the drainage direction from each DEM cell is restricted to only eight possibilities, separated by $\pi/4$ rad when square cells are used [*Fairfield and Leymarie*, 1991; *Quinn et al.*, 1991; *Costa-Cabral and Burges*, 1994], and (2) a drainage area which originates over a two-dimensional cell is treated as a point source (nondimensional) and is projected downslope by a line (one-dimensional) [*Moore and Grayson*, 1991]. To overcome these problems different alternative methods have been proposed in the literature [*Fairfield and Leymarie*, 1991; *Freeman*, 1991; *Quinn et al.*, 1991; *Lea*, 1992; *Costa-Cabral and Burges*, 1994; *Tarboton*, 1997]. All these methods mitigate some disadvantages of the D8 method but introduce new disadvantages as expressed by *Tarboton* [1997]. In particular, multiple drainage directions produce numerical dispersion of area from a DEM cell to all neighboring cells with a lower elevation, which may be inconsistent with the physical definition of upstream drainage area. In this respect, single drainage direction methods are nondispersive and they appear preferable. The method

proposed by *Tarboton* [1997] constitutes a reasonable compromise between the simplicity of the D8 method and the sophistication introduced in more recent formulations to improve the precision with which drainage directions are resolved by the D8 method. However, a certain degree of dispersion is maintained by Tarboton's method.

[3] In this paper, path-based methods are developed to mitigate the effects of grid artifacts affecting the D8 method while also avoiding randomness, dispersion, complex fitting surfaces, and significant computational costs [see *Tarboton*, 1997]. Bias arising from the selection of a single direction from each DEM cell is reduced by introducing cumulative (path-based) deviations between selected and theoretical drainage directions. Although this strategy does not eliminate the bias at the local level, it provides nonlocally constrained drainage paths which may improve significantly the nondispersive description of drainage systems. This is important in the field of terrain analysis applied to geomorphology and hydrology for three main reasons. First, dispersion of water may or may not occur in nature depending on the hydrologic circumstances, and multidirectional drainage may be an undesired numerical expedient in the description of transport phenomena occurring along well defined drainage paths (e.g., rivulet and channel flows, debris flows, or propagation of pollutants from a point source). Second, nondispersive methods are consistent with the physical definition of upstream drainage area, and this appears an essential requirement for the quantification of upstream releases (e.g., runoff, sediments, or pollutants from nonpoint sources) at given fluvial sections within (inhomogeneous) catchments. Finally, when nonlinear flow routing is used to describe surface and subsurface flows, the
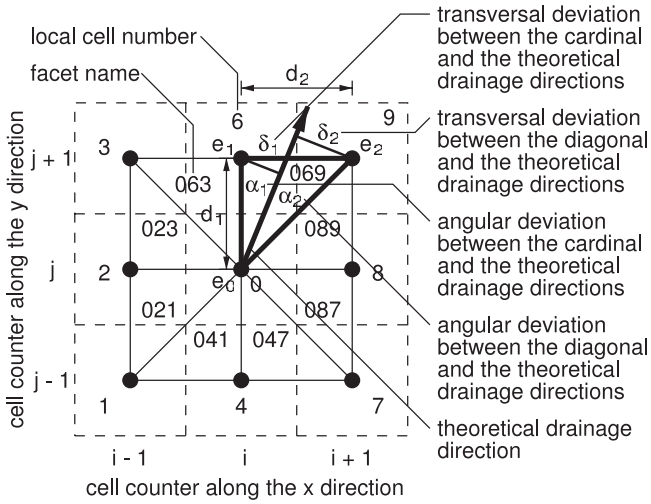
Figure 1. Sketch of the elementary computational system used in the D8-LAD and D8-LTD methods.

artificial dispersion of drainage paths may produce significant (and not easily controllable) alterations in the velocities of flows (which are nonlinearly dependent on flow discharge). This paper does not claim that nondispersive methods are always preferable with respect to (moderately) dispersive methods, but rather it aims to show that the classical D8 method can be improved significantly without introducing multiple drainage directions used in other more recent formulations.

2. Theory of Nondispersive Drainage

2.1. Determination of the Drainage Directions

2.1.1. Theoretical Drainage Directions

[4] The formulation developed by *Tarboton* [1997] is employed in this study to calculate the steepest (downward) drainage directions from any DEM cell of a catchment. These steepest drainage directions can vary continuously as an angle between 0 and 2π rad and are referred in this paper as theoretical drainage directions (TDDs). A sketch of the elementary computational system employed in this paper is shown in Figure 1. A block-centered representation is used with each elevation value taken to represent the elevation of the center of the corresponding cell. Eight planar triangular facets are formed between the cell and its eight neighboring cells. The three-dimensional geometry of each facet is characterized by the elevations e_i ($i = 0, 1, 2$) and by the distances d_i ($i = 1, 2$). The elevations are arranged such that e_0 is in the center point, e_1 is in the point to the side, and e_2

is in the diagonal point. For a generic triangular facet the slope (downward) can be represented by the vector (s_1, s_2), where $s_1 = (e_0 - e_1)/d_1$ and $s_2 = (e_1 - e_2)/d_2$. The direction (angle with the cardinal direction of the facet) and magnitude of the maximum slope in the facet are $r = \arctan(s_2/s_1)$ and $s_{\max} = (s_1^2 + s_2^2)^{1/2}$, respectively. If r is not in the angle range of the facet at the center point [0, $\arctan(d_2/d_1)$] ([0, $\pi/4$] rad when square cells are used), then r needs to be set as the direction along the appropriate edge and $s_{\max}$ assigned as the slope along the edge. If $r < 0$, then r and $s_{\max}$ are set equal to 0 and s_1, respectively. If $r > \arctan(d_2/d_1)$, then r and $s_{\max}$ are set equal to $\arctan(d_2/d_1)$ and $(e_0 - e_2)/(d_1^2 + d_2^2)^{1/2}$, respectively. Table 1 gives the node elevations corresponding to the corners of each of the triangular facets used to calculate slopes and angles. The TDD associated with a DEM cell is determined in the direction of the steepest downward slope on the eight triangular facets centered on that cell.

2.1.2. Local Analysis of Possible Drainage Directions

[5] The TDD calculated at a given DEM cell does not generally follow one of the cardinal (0, $\pi/2$, π, and $3\pi/2$ rad) or diagonal ($\pi/4$, $3\pi/4$, $5\pi/4$, and $7\pi/4$ rad when square cells are used) directions that can be selected. Possible drainage directions from a given DEM cell are identified using a pointer p which denotes the local cell number of the draining cell (Figure 1). More precisely, the pointers associated to the cardinal and diagonal directions of the facet containing the TDD are denoted p_1 and p_2, respectively (Table 1). A possible criterion for approximating the TDD with a single drainage direction is to ensure the least angular deviation (LAD). As shown in Figure 1, the angular deviations produced when approximating the TDD by the cardinal and the diagonal directions are α_1 and α_2, respectively, where $\alpha_1 = r$ and $\alpha_2 = \arctan(d_2/d_1) - r$ ($\pi/4 - r$ rad when square cells are used). The LAD criterion determines that the direction identified by p_1 is selected if $\alpha_1 \leq \alpha_2$, whereas the direction identified by p_2 is selected if $\alpha_1 > \alpha_2$. One can note that the slope along the cardinal and diagonal directions display the same value if the direction of the maximum slope is $r = \arctan(d_2/d_1)/2$ ($\pi/8$ rad when square cells are used). Hence the slope along the cardinal direction is greater than the slope along the diagonal direction if $r < \arctan(d_2/d_1)/2$, whereas the opposite situation occurs if $r > \arctan(d_2/d_1)/2$. Therefore the LAD criterion determines the possible direction with the steepest (downward) slope and reproduces the classical D8 method.

[6] An alternative strategy is considered here by introducing the criterion of the least transversal deviation (LTD). The transversal deviation is defined here as the linear distance between the center of the draining cell and the path along the TDD that originates at the center of the drained cell. As shown in Figure 1, the transversal deviations produced when

Table 1. Factors for the Calculation of Drainage Directions and Deviations at Any Triangular Facet

	Facet Name in Figure 1							
Factor	021	023	063	069	089	087	047	041
e_0	$e_{i,j}$	$e_{i,j}$	$e_{i,j}$	$e_{i,j}$	$e_{i,j}$	$e_{i,j}$	$e_{i,j}$	$e_{i,j}$
e_1	$e_{i-1,j}$	$e_{i-1,j}$	$e_{i,j+1}$	$e_{i,j+1}$	$e_{i+1,j}$	$e_{i+1,j}$	$e_{i,j-1}$	$e_{i,j-1}$
e_2	$e_{i-1,j-1}$	$e_{i-1,j+1}$	$e_{i-1,j+1}$	$e_{i+1,j+1}$	$e_{i+1,j+1}$	$e_{i+1,j-1}$	$e_{i+1,j-1}$	$e_{i-1,j-1}$
p_1	2	2	6	6	8	8	4	4
p_2	1	3	3	9	9	7	7	1
σ	+1	−1	+1	−1	+1	−1	+1	−1

approximating the TDD by the cardinal and the diagonal directions are $\delta_1 = d_1 \sin \alpha_1$ and $\delta_2 = (d_1^2 + d_2^2)^{1/2} \sin \alpha_2$, respectively. The LTD criterion determines that the direction identified by p_1 is selected if $\delta_1 \leq \delta_2$, whereas the direction identified by p_2 is selected if $\delta_1 > \delta_2$. Note that the LTD and LAD criteria are not equivalent as $\alpha_1 \neq \alpha_2$ for $\delta_1 = \delta_2$. When square cells are used ($d_1 = d_2$), one can obtain that $\delta_1 = \delta_2$ for $r = 0.4636$ rad ($26.56°$), which is significantly greater than $\pi/8$ rad ($22.50°$). The LTD criterion appears as realistic as the LAD criterion. The former highlights the deviations at the end of the elemental drainage paths, while the latter at the beginning (Figure 1). Both the LAD and LTD criteria are employed in this study to formulate two classes of methods for the determination of nondispersive drainage directions. These classes of methods are designated here D8-LAD (eight drainage directions, least angular deviation) and D8-LTD (eight drainage directions, least transversal deviation), respectively.

2.1.3. Path-Based Analysis of Possible Drainage Directions

[7] In the D8-LAD and D8-LTD methods, a single drainage direction from each DEM cell is selected among the eight possible directions by considering the angular or transversal deviations, respectively, both at the local computational scale depicted in Figure 1 and along the upstream drainage path. A sign σ is assigned to each deviation that may occur in the eight triangular facets of the elementary computational system so as to allow a meaningful (arithmetic) accumulation of deviations along a drainage path. Possible values of p_1, p_2 and σ are reported in Table 1. For any DEM cell, the values of r, s_{max}, p_1, p_2, and σ for the facet containing the TDD are calculated by considering the eight facets centered on that DEM cell. The accumulation of deviations along a drainage path is formulated in this section by considering the transversal deviations (D8-LTD methods). A similar formulation can be easily derived for the case in which angular deviations are considered (D8-LAD methods).

[8] At the kth cell along a given path ($k = 1, 2, \ldots$), the local transversal deviations associated to pointers p_1 and p_2 are $\delta_1(k) = d_1 \sin \alpha_1$, where $\alpha_1 = r$, and $\delta_2(k) = (d_1^2 + d_2^2)^{1/2} \sin \alpha_2$, where $\alpha_2 = \arctan(d_2/d_1) - r$ ($\pi/4 - r$ rad when square cells are used), respectively. The related cumulative transversal deviations are defined here as $\delta_1^+(k) = \sigma\delta_1(k)$ and $\delta_2^+(k) = -\sigma\delta_2(k)$, for $k = 1$, or as

$$\delta_1^+(k) = \sigma\,\delta_1(k) + \lambda\,\delta^+(k-1) \qquad (1)$$

and

$$\delta_2^+(k) = -\sigma\,\delta_2(k) + \lambda\,\delta^+(k-1), \qquad (2)$$

for $k = 2, 3, \ldots$, where λ is a dampening factor that can assume values varying between 0 and 1. The drainage direction is selected between the two possibilities so as to minimize the absolute value of the cumulative transversal deviation $\delta^+(k)$ ($k = 1, 2, \ldots$).

$$\text{If } \left|\delta_1^+(k)\right| \leq \left|\delta_2^+(k)\right|, \ \delta^+(k) = \delta_1^+(k), \ p = p_1. \qquad (3)$$

$$\text{If } \left|\delta_1^+(k)\right| > \left|\delta_2^+(k)\right|, \ \delta^+(k) = \delta_2^+(k), \ p = p_2. \qquad (4)$$

For $\lambda = 0$, the selection of the drainage directions is based only on the local transversal deviations $\delta_1(k)$ and $\delta_2(k)$ ($k = 1, 2, \ldots$). For $0 < \lambda \leq 1$ the memory of the upstream transversal deviations between selected and theoretical drainage directions is retained. For $\lambda = 1$, full memory of the upstream transversal deviations is retained. For $0 < \lambda < 1$, the upstream transversal deviations are dampened proceeding downstream. The D8-LAD methods are expressed by equations similar to those reported in this paragraph, where angular deviations are considered in preference to transversal deviations (section 2.1.2).

[9] One can note that the D8-LAD method with $\lambda = 0$ reproduces the classical D8 method. It is also remarked here that the benefit of using cumulative (path-based) deviations for the determination of drainage directions can be demonstrated geometrically only if the D8-LTD method with $\lambda = 1$ and the simple case of a planar slope are considered. In the case of the planar slope, one can verify that the D8-LAD method (with $\lambda = 1$) produces nonlocally biased drainage paths as these paths become sufficiently long. Nevertheless, both angular and transversal deviations are employed in this study and the resulting D8-LAD and D8-LTD methods are evaluated numerically considering also complex drainage systems.

2.2. Calculation of the Drainage Areas

[10] The algorithm that incorporates the D8-LAD and D8-LTD methods for identifying the drainage network and calculating the drainage areas within a catchment requires three preliminary operations, in which (1) DEM cells of the catchment are sorted into descending elevation order, (2) a recursive procedure is used to raise the elevations of the cells located in flat or depressed areas so as to ensure a drainage direction with a small positive slope (downward) for all the cells of the catchment, and (3) DEM cells are sorted again into descending elevation order. The D8-LAD or the D8-LTD method is then applied to form the drainage network and to calculate the drainage areas. DEM cells are processed in the order of descending elevation. For cells where multiple paths converge, the cumulative deviation is calculated by considering the path with the largest upstream drainage area. Upstream drainage areas are summed up over all the drained cells. The algorithm described in this section appears as general and efficient as the climbing recursive algorithm developed by *Mark* [1988] and *Tarboton* [1997].

3. Study Cases

3.1. Synthetic Drainage Systems

[11] Four synthetic drainage systems are considered: a planar slope, a spherical mountain, a spherical crater, and a parabolic valley. Three-dimensional visualizations of these drainage systems are shown in Figures 2a–2d. Drainage networks extracted using the D8-LAD method with $\lambda = 0$ and the D8-LTD method with $\lambda = 1$ are shown in Figures 2e–2h and 2i–2l, respectively. The capabilities of the D8-LAD and D8-LTD methods are evaluated in this section by monitoring the relative error $\epsilon_A = (A - A_t)/A_t$ between calculated (A) and theoretical (A_t) drainage areas. Calculated drainage areas A are obtained numerically from the algorithm described in section 2.2, whereas theoretical drainage areas A_t are obtained using the analytical integrals of the drainage lines through the corners of the draining cells.
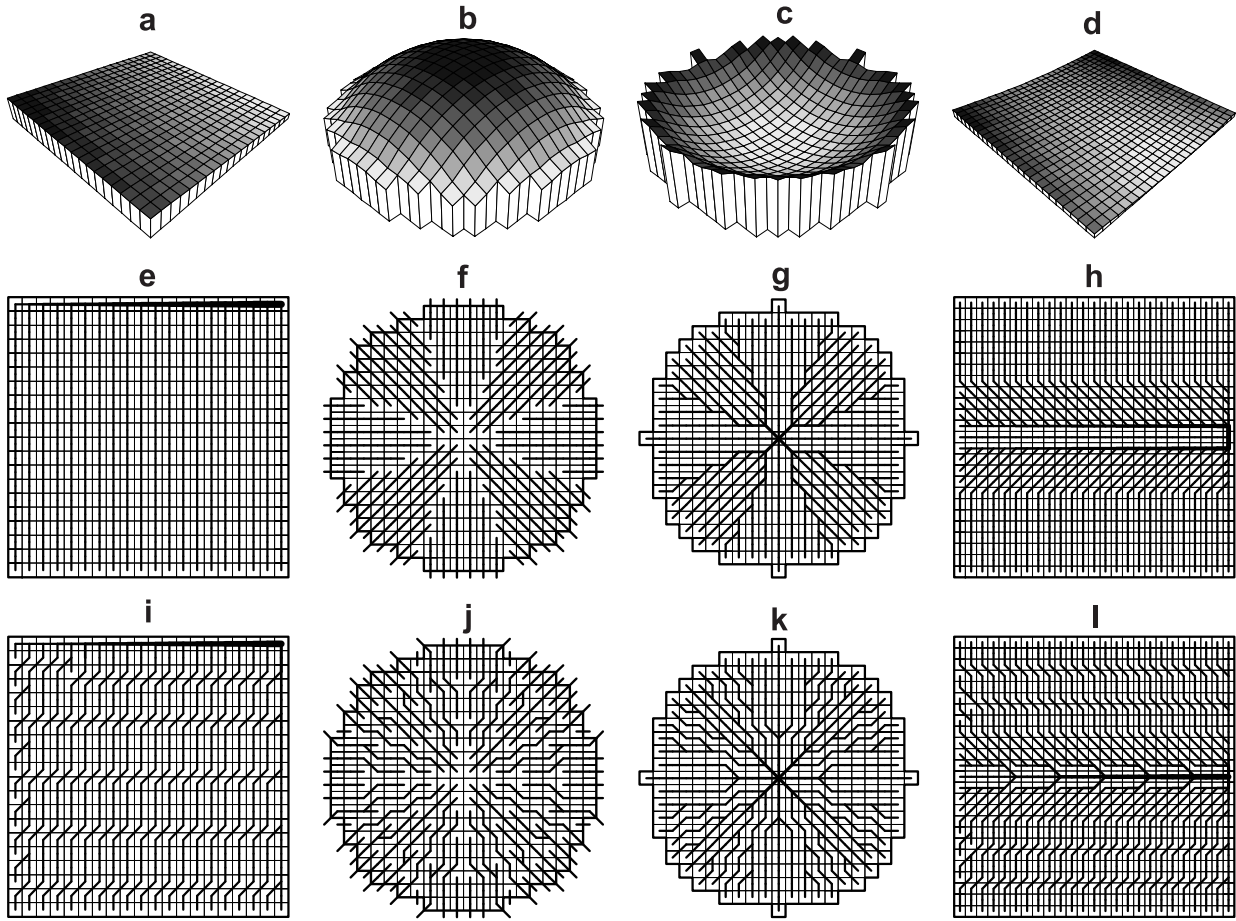
Figure 2.   Synthetic drainage systems: (a) planar slope, (b) spherical mountain, (c) spherical crater, and (d) parabolic valley. Drainage paths determined using (e–h) the D8-LAD method with $\lambda = 0$ and (i–l) the D8-LTD method with $\lambda = 1$.

Three error functions of ϵ_A are used to express the average performance of the D8-LAD and D8-LTD methods across a drainage system: the mean error (ME), the mean absolute error (MAE), and the root-mean square error (RMSE). The ME is defined as ME = $E[\epsilon_A]$, where $E[\cdot]$ is the expected value of $[\cdot]$, and expresses the bias between calculated and theoretical drainage areas. The MAE is defined as MAE = $E[|\epsilon_A|]$ and expresses the mean absolute deviation between calculated and theoretical drainage areas. The RMSE is defined as RMSE = $(E[\epsilon_A^2])^{1/2}$ and expresses a deviation between calculated and theoretical drainage areas as well as the MAE, but it emphasizes the outliers in ϵ_A.

[12]   Numerical experiments are conducted to determine the optimal value of the dampening factor λ. ME, MAE, and RMSE are calculated over all the DEM cells of each drainage system. The variations of these error functions with λ are plotted in Figure 3. Overall, the obtained results can be summarized as follows. In the cases of the planar slope and of the parabolic valley, MAE and RMSE decrease as λ increases. This indicates that the memory of upstream deviations (either angular or transversal) is important to provide accurate descriptions of the drainage networks. The decay of MAE and RMSE with increasing λ occurs earlier for the D8-LAD method than for the D8-LTD method, but the values of MAE and RMSE displayed at $\lambda = 1$ are

essentially the same for the two methods. In the cases of the spherical mountain and of the spherical crater, MAE and RMSE are almost constant as λ increases. This indicates that, in these two cases, when the average performance of the methods are evaluated over all the DEM cells of the drainage systems, the D8-LAD and D8-LTD methods offer no significant improvements with respect to the classical D8 method. Finally, the ME at $\lambda = 1$ is negative for all the cases and this can be referred to the restriction (2) of the D8 method mentioned in section 1.

[13]   There are further aspects of the developed methods that can be emphasized numerically by considering the variations in the relative error ϵ_A at selected transects transversal to the mainstream (in the cases of the planar slope and of the parabolic valley) or at selected arcs of contour line (in the cases of the spherical mountain and of the spherical crater). An example is shown in Figure 4, where the relative errors ϵ_A between calculated and theoretical areas drained by selected arcs in the spherical mountain are considered. Each arc is characterized by an aperture γ of about 3/15 rad (24°) and an axis orientation angle θ. The error ϵ_A plotted in Figure 4 expresses the relative difference between calculated and theoretical areas drained globally by all the DEM cells used to describe a selected arc. The variations of ϵ_A with θ are plotted for the D8-LAD method
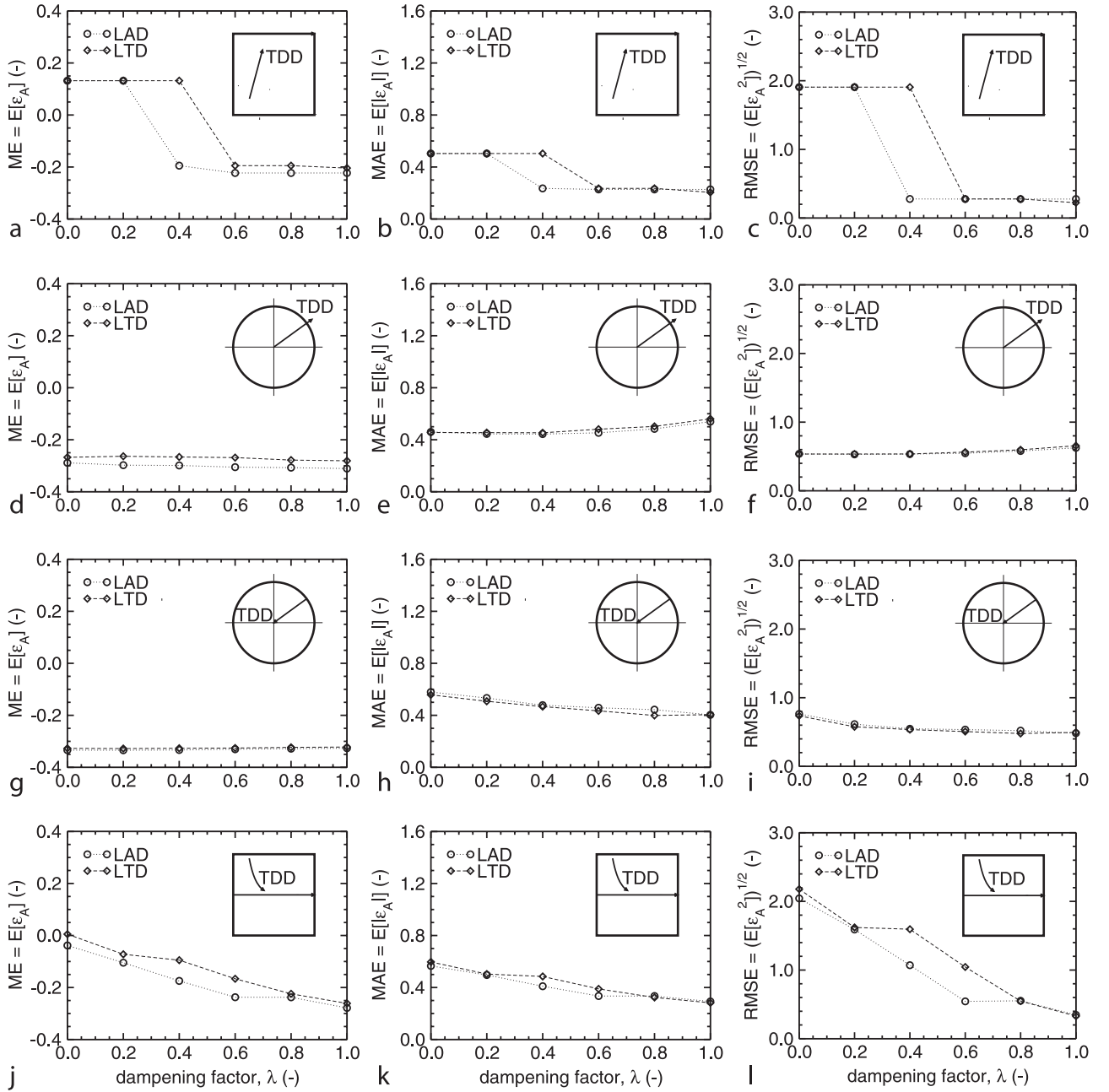
Figure 3. Variations of the mean error (ME), mean absolute error (MAE), and root-mean square error (RMSE) of ϵ_A for variable values of the dampening factor λ. ME, MAE, and RMSE are calculated for the D8-LAD and D8-LTD methods, over all the DEM cells of the planar slope (Figures 3a, 3b, and 3c, respectively), of the spherical mountain (Figures 3d, 3e, and 3f, respectively), of the spherical crater (Figures 3g, 3h, and 3i, respectively), and of the parabolic valley (Figures 3j, 3k, and 3l, respectively).

with $\lambda = 0$, for the D8-LAD method with $\lambda = 1$, and for the D8-LTD method with $\lambda = 1$. The results shown in Figure 4 reveal that a significant improvement is obtained using the D8-LTD method with $\lambda = 1$ in preference to the D8-LAD method with $\lambda = 0$. A slight improvement is also obtained with respect to the D8-LAD method with $\lambda = 1$. These results are not contrasting with those shown in Figures 3. The spherical mountain is intrinsically dispersive and thus it can not be described accurately at all the DEM cells using either the D8-LAD and D8-LTD methods (Figures 3d–3f). However, as shown in Figures 2 and 4, the consideration of

cumulative (path-based) deviations allows reproductions of drainage paths that are nonlocally unbiased with respect to grid orientation and, within the limitations imposed by nondispersive drainage, reasonably accurate.

[14] Other important issues are connected to the occurrence of errors in DEM data. These issues are studied in this paper by performing a Monte Carlo analysis of the results produced by the D8-LAD and D8-LTD methods over the synthetic drainage systems when DEM data are artificially perturbed. The case of the spherical mountain is reported. Normal deviates with zero mean and assigned standard
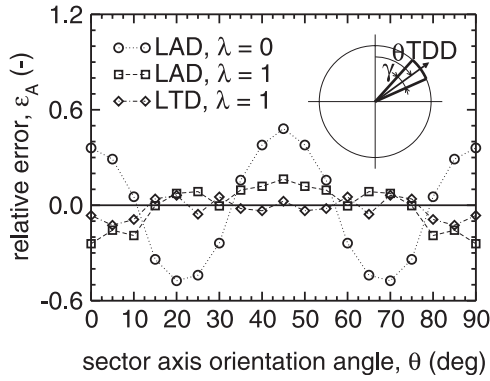
Figure 4. Variation of the relative error ϵ_A at arcs with aperture γ of about 3/15 rad (24°) selected in the spherical mountain, for variable sector axis orientation angle θ.

deviation σ_ζ are applied to each DEM cell of size Δx. The responses of the D8-LAD and D8-LTD methods are evaluated in terms of RMSE of ϵ_A over all the DEM cells (Figure 5a), and in terms of relative error ϵ_A at a selected arc with aperture $\gamma = 3/15$ rad (24°) and axis orientation angle $\theta = \pi/4$ rad (Figure 5b). As shown in Figure 5a, when the DEM data are affected by errors with $\sigma_\zeta/\Delta x$ less than about 5%, the D8-LAD method with $\lambda = 0$ provides better average reproductions of the drainage areas than the D8-LTD method with $\lambda = 1$. For $\sigma_\zeta/\Delta x$ greater than about 5%, the D8-LAD and D8-LTD methods may produce comparable results. However, as shown in Figure 5b, when the area
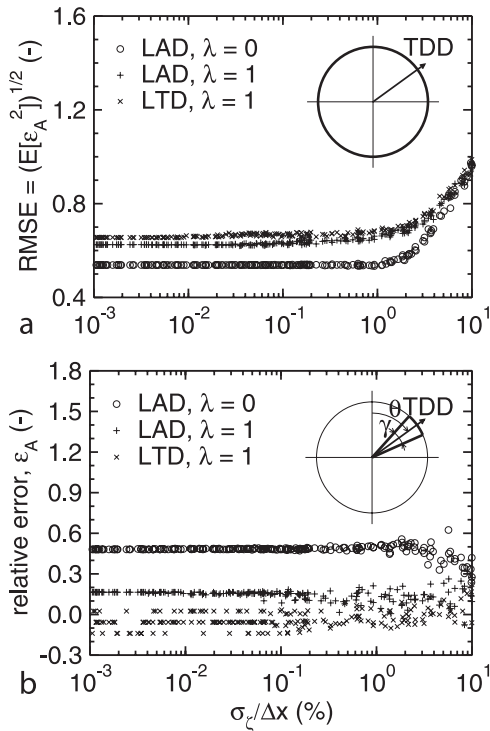
Figure 5. Monte Carlo analysis of the errors connected to the application of the D8-LAD and D8-LTD methods to the spherical mountain, when DEM data of resolution Δx are perturbed with normal deviates of zero mean and standard deviation σ_ζ.
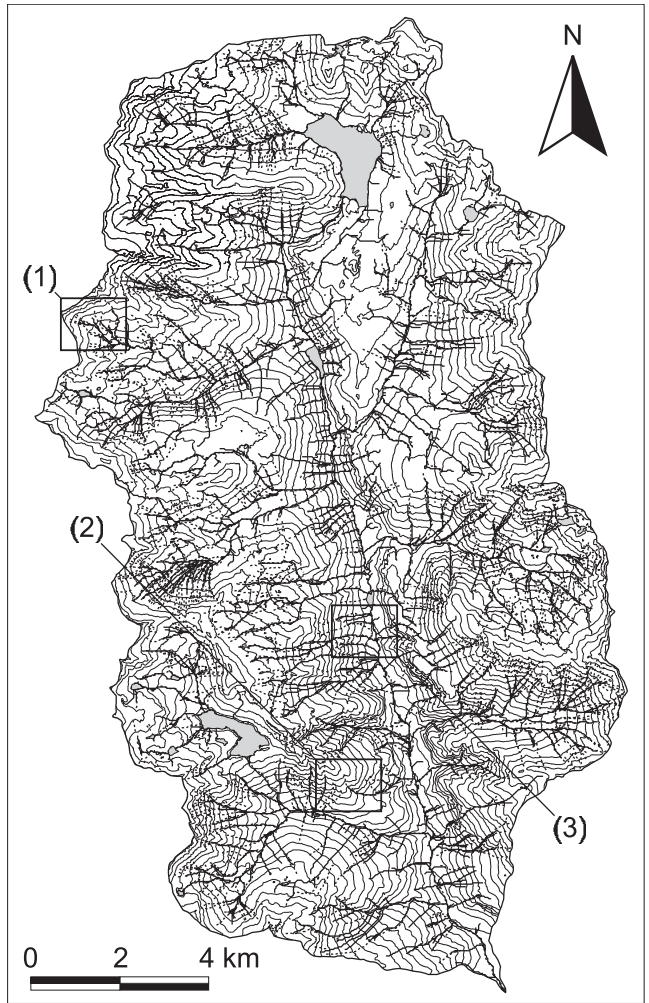

Figure 6. Contour map of the Liro catchment. The contour interval is 100 m. Shaded areas denote the lakes in the Liro catchment. Drainage paths reproduced using the D8-LTD method with $\lambda = 1$ and DEM data at 30-m resolution (solid lines) are plotted along with contour lines and cartographic blue lines (dashed lines). Rectangles (1), (2), and (3) denote the areas selected to provide insets that zoom in the catchment area (Figure 7).

drained by the selected arc is considered and when $\sigma_\zeta/\Delta x$ is less than about 5%, the D8-LAD method with $\lambda = 0$ is significantly improved by the D8-LAD and D8-LTD methods with $\lambda = 1$. For $\sigma_\zeta/\Delta x$ greater than about 5%, the results provided by the examined methods tend to become comparable. One can note that the performance of the D8-LAD method with $\lambda = 0$ improves as σ_ζ increases. Errors in the DEM data tend to produce erratic drainage paths which distributes almost equally the drained area along the lower draining circumference. This effect is clearly accidental but needs to be taken into consideration when assessing the results obtained in the case of the spherical mountain.

3.2. Liro Catchment

[15] The Liro catchment is located in the central Italian Alps, near the town of Chiavenna, and has an extension of approximately 193 km². Planimetric and relief features of the Liro catchment are shown in the map reported in
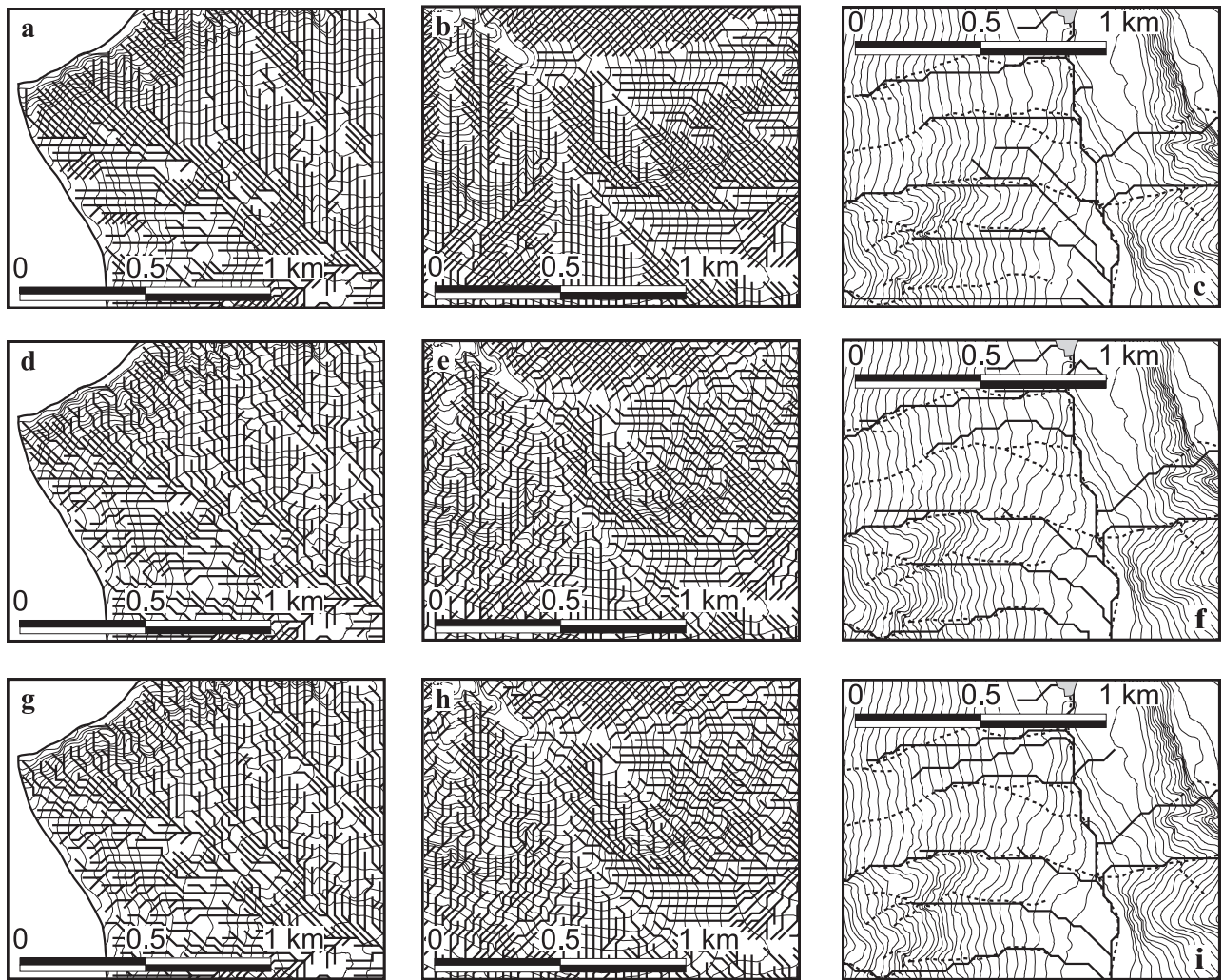
Figure 7. Insets that zoom in the Liro catchment area corresponding to the rectangles (1), (2), and (3) indicated in Figure 6 and to the application of the D8-LAD method with $\lambda = 0$ (Figures 7a, 7b, and 7c, respectively), of the D8-LAD method with $\lambda = 1$ (Figures 7d, 7e, and 7f, respectively), and of the D8-LTD method with $\lambda = 1$ (Figures 7g, 7h, and 7i, respectively). Reproduced drainage paths (solid lines) are plotted along with contour lines and cartographic blue lines (dashed lines, only for Figures 7c, 7f, and 7i). The contour interval is 25 m.

Figure 6. The terrain is mountainous, with average elevation of about 1960 m above sea level (asl). The elevation of the highest peak is approximately 3278 m asl, and the outlet is at about 300 m asl. DEM data at 30-m resolution are obtained from topographic cartography on a scale of 1:10,000 (Italian CTR cartography) by conversion of printed contour lines and height spots. The quality of these data was tested using the five basic criteria described by *Carrara et al.* [1997]. The resulting contour error was found to be approximately 5% of the contour interval employed on the CTR cartography (10 m). The capabilities of the D8-LAD and D8-LTD methods are evaluated in this section by examining visually extracted drainage paths, reproduced contour lines, and cartographic blue lines. Although the use of direct surveys of land surface and channels would allow a more meaningful analysis, the data used in this study appear sufficiently accurate to provide useful indications on the features that the developed methods display in real catchment applications.

[16] The drainage networks extracted using the D8-LAD method with $\lambda = 0$, the D8-LAD method with $\lambda = 1$, and the D8-LTD method with $\lambda = 1$ are considered. Results are reported in Figures 6 and 7. Figure 6 shows the drainage network extracted over the entire catchment area (using the D8-LTD method with $\lambda = 1$) and the three rectangles selected to provide insets that zoom in the catchment area ((1), (2), and (3)). Figure 7 shows the drainage networks extracted over these three rectangles using the D8-LAD method with $\lambda = 0$ (Figures 7a–7c, respectively), the D8-LAD method with $\lambda = 1$ (Figures 7d–7f, respectively), and the D8-LTD method with $\lambda = 1$ (Figures 7g–7i, respectively). A critical support area of 0.054 km^2 is used for drainage paths visualization in Figure 6 and in Figures 7c, 7f, and 7i. One can note that the D8-LAD and D8-LTD methods with $\lambda = 1$ reproduce the drainage paths over hillslope areas significantly better than the D8-LAD method with $\lambda = 0$ (Figures 7a–7b, 7d–7e, and 7g–7h). When upstream deviations are considered ($\lambda = 1$), the resulting drainage paths

appear satisfactorily consistent with the related land surface topography. This can be inferred by noting that the reproduced drainage paths are, at least in their average courses, reasonably normal to the contour lines. When upstream deviations are not considered ($\lambda = 0$), the resulting drainage paths appear clearly affected by grid orientation and form patterns characterized by parallel lines. Along the valleys, the D8-LTD method with $\lambda = 1$ appears to provide significantly better results than the D8-LAD method with $\lambda = 0$ (Figures 7c and 7i). A certain improvement is also observed with respect to the D8-LAD method with $\lambda = 1$ (Figures 7f and 7i). This is likely to reflect the fact that transversal deviation are geometrically more appropriate than angular deviations for the process of (arithmetic) accumulation along drainage paths as mentioned in section 2.1.

4.   Concluding Remarks

[17]   The applications of the D8-LAD and D8-LTD methods conducted in section 3 reveal that the use of cumulative (path-based) deviations between selected and theoretical drainage directions is important to provide accurate descriptions of the drainage paths both over hillslope areas and along the valleys (Figures 2, 6, and 7). In addition, the consideration of transversal deviations in preference to angular deviations appears beneficial to allow accurate reproductions of long drainage paths such as those that reach the valleys (Figures 7f and 7i). In essence, improvements over the classical D8 method (D8-LAD method with $\lambda = 0$) are produced, firstly, by introducing cumulative (path-based) deviations between selected and theoretical drainage directions (D8-LAD and D8-LTD methods with $\lambda = 1$) and, secondly, by using transversal deviations in preference to angular deviations (D8-LTD method with $\lambda = 1$). Hence the D8-LTD method with $\lambda = 1$ is advocated and it can be referred to as the D8-LTD method when no specification for λ is made. The D8-LTD method warrants consideration in distributed catchment modeling, especially when artificial dispersion is not desirable.

5.   Availability

[18]   The Fortran codes that implement the procedures presented in this paper are available upon request from the first author.

References

Carrara, A., G. Bitelli, and R. Carlà, Comparison of techniques for generating digital terrain models from contour lines, *Int. J. Geogr. Inf. Sci.*, *11*, 451–473, 1997.

Costa-Cabral, M., and S. J. Burges, Digital elevation model networks (DEMON): A model of flow over hillslopes for computation of contributing and dispersal areas, *Water Resour. Res.*, *30*, 1681–1692, 1994.

Fairfield, J., and P. Leymarie, Drainage networks from grid digital elevation models, *Water Resour. Res.*, *27*, 709–717, 1991.

Freeman, T. G., Calculating catchment area with divergent flow based on a regular grid, *Computat. Geosci.*, *17*, 413–422, 1991.

Lea, N. L., An aspect driven kinematic routing algorithm, in *Overland Flow: Hydraulics and Erosion Mechanics*, edited by A. J. Parsons and A. D. Abrahams, pp. 393–407, Chapman and Hall, New York, 1992.

Mark, D. M., Network models in geomorphology, in *Modelling in Geomorphological Systems*, edited by M. G. Anderson, pp. 73–97, John Wiley, New York, 1988.

Marks, D., J. Dozier, and J. Frew, Automated basin delineation from digital elevation data, *GeoProcessing*, *2*, 299–311, 1984.

Moore, I. D., and R. B. Grayson, Terrain-based catchment partitioning and runoff prediction using vector elevation data, *Water Resour. Res.*, *27*, 1177–1191, 1991.

O'Callaghan, J., and D. M. Mark, The extraction of drainage networks from digital elevation data, *Comput. Vision Graph.*, *28*, 323–344, 1984.

Quinn, P., K. Beven, P. Chevallier, and O. Planchon, The prediction of hillslope flow paths for distributed hydrological modeling using digital terrain models, *Hydrol. Processes*, *5*, 59–80, 1991.

Tarboton, D. G., A new method for the determination of flow directions and upslope areas in grid digital elevation models, *Water Resour. Res.*, *33*, 309–319, 1997.

————————————

M. Franchini, G. Moretti, and S. Orlandini, Dipartimento di Ingegneria, Università degli Studi di Ferrara, Via Saragat 1, I-44100 Ferrara, Italy. (stefano.orlandini@unife.it)

B. Aldighieri and B. Testa, Istituto per la Dinamica dei Processi Ambientali, Consiglio Nazionale delle Ricerche, Piazza della Scienza 4, I-20126 Milano, Italy.